Suppression of the centrifugal barrier effects in the off-energy-shell neutron + ^{17}O interaction

M. Gulino,[1,2] C. Spitaleri,[1,3] X. D. Tang,[4] G. L. Guardo,[1,3] L. Lamia,[1,3] S. Cherubini,[1,3] B. Bucher,[4] V. Burjan,[5] M. Couder,[4] P. Davies,[4] R. deBoer,[4] X. Fang,[4] V. Z. Goldberg,[6] Z. Hons,[5] V. Kroha,[5] L. Lamm,[4,*] M. La Cognata,[1] C. Li,[7] C. Ma,[4] J. Mrazek,[5] A. M. Mukhamedzhanov,[6] M. Notani,[4] S. O'Brien,[4] R. G. Pizzone,[1] G. G. Rapisarda,[1,3] D. Roberson,[4] M. L. Sergi,[1,3] W. Tan,[4] I. J. Thompson,[8] and M. Wiescher[4]

[1]*INFN Laboratori Nazionali del Sud, Catania, Italy*
[2]*Università degli Studi di Enna "KORE", Enna, Italy*
[3]*Dipartimento di Fisica ed Astronomia, Università degli Studi di Catania, Catania, Italy*
[4]*Department of Physics, Joint Institute for Nuclear Astrophysics, University of Notre Dame, Indiana, USA*
[5]*Nuclear Physics Institute of ASCR, Rez, Czech Republic*
[6]*Cyclotron Institute, Texas A&M University, College Station, Texas, USA*
[7]*China Institute of Atomic Energy, Beijing, China*
[8]*Lawrence Livermore National Laboratory, Livermore, California, USA*

The reaction ^{17}O$(n, \alpha)^{14}$C was studied at energies from $E_{c.m.} = 0$ to $E_{c.m.} = 350$ keV by using the quasifree deuteron breakup in the three-body reaction ^{17}O $+ d \rightarrow \alpha + {}^{14}$C $+ p$, which extended the Trojan Horse indirect method (THM) to neutron-induced reactions. It is found that the ^{18}O excited state at $E^* = 8.125 \pm 0.002$ MeV, observed in THM experiments, is absent in the direct measurement because of its high centrifugal barrier. The angular distributions of the populated resonances have been measured by using this method. The results unambiguously indicate the ability of the THM to overcome the centrifugal barrier suppression effect and to pick out the contribution of the bare nuclear interaction.

PACS number(s): 25.40.−h, 28.20.−v, 26.90.+n

In the past decade, to extract the cross sections of two-body reactions at low energies for astrophysical applications, many indirect methods have been developed. Among them, the Trojan Horse method (THM) [1–7] has been applied successfully to the study of several charged-particle-induced reactions bypassing the Coulomb barrier penetration effect and the electron screening effect dominant at very low energies. Briefly, in the THM, the cross section of the $A + x \rightarrow C + c$ reaction is determined by measuring the differential cross section of a suitable reaction $A + a \rightarrow C + c + s$ and by selecting the events where the Trojan Horse (TH) nucleus a, which has a strong $x \oplus s$ cluster structure, breaks up inside the nuclear field of nucleus A. This process is most likely inside the quasifree (QF) kinematics regime, i.e., when the momentum transfer to the spectator (the cluster s of the TH nucleus) is small. Hence, if the wave function of the intercluster motion is dominated by the $l = 0$ component, as for the deuteron, the relative momentum p_{xs} of the clusters x and s of the TH nucleus is close to zero. In the center of mass of the A-x system, the two-body reaction $A + x \rightarrow C + c$ takes place at the energy given in the postcollision prescription by $E_{c.m.} = E_{Cc} - Q_2$, where E_{Cc} is the relative energy of the ejectiles and Q_2 is the Q value of the two-body reaction $A + x \rightarrow C + c$. Consequently, the energy $E_{c.m.}$ can lie below the Coulomb barrier, even if the reaction $A + a$ occurs at an energy above the barrier.

The application of the THM to the indirect study of p-p scattering has strongly confirmed the THM hypothesis, i.e., the suppression of Coulomb effects in the two-body cross section

at sub-Coulomb energies [4]. Indeed, the deep minimum in the p-p scattering cross section, due to the interference between nuclear and Coulomb diffusion amplitudes, is missing in the TH data because of the suppression of the Coulomb contribution, which results from this method [4].

In the present Rapid Communication, the ability of the THM to overcome the centrifugal barrier effects is definitely and unambiguously demonstrated by studying a neutron-induced two-body reaction, which does not suffer Coulomb hindrance. To perform this measurement, the deuteron QF breakup is used as a source of virtual neutrons [8].

The two-body reaction ^{17}O $+ n \rightarrow {}^{14}$C $+ \alpha$ has been chosen to investigate the effect of centrifugal barrier suppression. This reaction is interesting for both nuclear energy and nuclear astrophysics. In fact, in nuclear reactors, the neutron-induced reactions on ^{14}N and ^{17}O are the dominant sources of the radioactive isotope ^{14}C ($T_{1/2} = 5730$ yr) [9]. In nuclear astrophysics, this reaction takes place in the nucleosynthesis of heavier elements in various astrophysical scenarios [10,11], and it could help to explain anomalies in ^{18}O/^{16}O and ^{17}O/^{16}O ratios found in asymptotic giant branch stars and in circumstellar Al$_2$O$_3$ meteorite grains [12].

For incident-neutron energies from thermal up to a few hundred keV, the cross section of this reaction is characterized by the presence of several narrow resonant states in the ^{18}O compound nucleus. Three resonances have energies above the ^{17}O $+ n$ threshold (8044 keV), and one subthreshold level is present. The resonance parameters are reported in Table I. The total width (Γ_{tot}) for each resonance from the literature together with the relevant references are presented in the last two columns of the table. For the negative-energy resonance, the reduced width is given.

TABLE I. Summary of the ^{18}O resonance parameters in the energy range explored by the experiment. For the negative-energy resonance, the reduced width (rw) is given.

E^* (keV)	$E_{c.m.}$ (keV)	J^π	Γ_{tot} (keV)	Reference
8038 ± 0.7	-7	1^-	< 2.5 (rw)	[13]
			2.4 (rw)	[14]
8125 ± 2	75	5^-		
8213 ± 4	166	2^+	1.0 ± 0.8	[13]
			1.280 ± 1.000	[15]
			2.258 ± 0.135	[14]
8282 ± 3	236	3^-	8.0 ± 1.0	[13]
			8.000 ± 1.000	[15]
			14.739 ± 0.590	[14]

Direct measurements [14–20] have shown the population of the two excited states at energies 8213 and 8282 keV and the influence of the subthreshold level at 8038 keV. At the astrophysical relevant temperatures ($T \in [0.01 - 1.3] \times 10^9$ K), the reaction rate calculated by using the different data sets [14–16] differs by a factor of 2–2.5 with a consequent change in the abundance ratios for some elements (e.g., ^{22}Ne, ^{26}Mg) [10].

The 8125-keV state of ^{18}O would be populated by f-wave neutrons, but due to the high orbital momentum barrier, the cross section is too low for direct measurement.

Since the THM should not be affected by orbital momentum barrier effects, we anticipate that the three-bodies ^{2}H(^{17}O, $\alpha\,^{14}$C)^{1}H study should provide observational evidence for resonance contributions from all known states.

Two experiments were performed: the first one at the Laboratori Nazionali del Sud (LNS) in Catania, Italy and the second one at the Nuclear Science Laboratory (NSL) of the University of Notre Dame, IN, USA. In the LNS experiment, a ^{17}O beam of 41 MeV was delivered onto a CD$_2$ target of thickness 150 μg/cm^2. In the NSL experiment, a beam energy of 43.5 MeV and a target thickness of 170 μg/cm^2 were used.

The angles and the energies of the ejectiles α and ^{14}C were detected in coincidence by using an experimental setup, symmetric with respect to the beam axis, which consists of six position-sensitive silicon detectors [(PSDs), single area, resistive readout, spatial resolution 0.5 mm]. The proton was not detected in these experiments, and its energy and angle were reconstructed from kinematical calculations. The PSD detectors covered the angular ranges in the laboratory reference system $\theta_1 = 5°–10°$, $\theta_2 = 13.3°–20.8°$, and $\theta_3 = 21.5°–29.0°$ in the LNS experiment and $\theta_1 = 5°–10°$, $\theta_2 = 13.1°–18.1°$, and $\theta_3 = 23.8°–28.8°$ in the NSL experiment. The two most forward detectors were equipped with ionization chambers used as ΔE detectors to identify carbon. Coincidences among either one of the two forward PSD detectors and one of the three placed on the opposite side with respect to the beam axis were recorded by the data acquisition system.

The reaction of interest was identified by selecting events in which a carbon was detected in one of the telescopes. The reconstructed Q value for the three-body reaction ($Q = -0.6 \pm 0.3$ MeV) is in agreement with the expected one ($Q = -0.407$ MeV).

The beam energy was chosen such that (i) the incident center-of-mass energy (after half target thickness $E_{c.m.} = 4.27$ MeV in the LNS experiment and $E_{c.m.} = 4.53$ MeV in the NSL experiment) was higher than the binding energy of n and p in d ($B_{xs} = 2224.5 \pm 0.2$ keV), and (ii) the wavelength in the entrance channel ($\lambda = 1.65$ fm in the LNS experiment and $\lambda = 1.60$ fm in the NSL experiment) was smaller than the deuteron radius ($r_d = 4.5$ fm). As a result, the validity conditions of the impulse approximation (IA) approach remained fulfilled.

By following the procedure described elsewhere [1–8], many tests have been performed to ensure the presence of the QF reaction mode and to establish ways to discriminate from other reaction contributions, which populate the same final state. The strongest evidence of the predominance of the QF mechanism is given by the shape of the momentum distribution for the p-n intercluster motion in the deuteron. This was extracted by using the standard procedure, which selects events that correspond to the most populated resonance in the TH measurement at an energy of 8213 keV. The result is shown in Fig. 1 by black dots for the LNS experiment and open squares for the NSL experiment. The solid line in Fig. 1 represents the Hulthén function in momentum space with the standard parameter values [5–8] ($\tilde{\chi}^2 = 1.45$). This is expected if the plane-wave IA (PWIA) is used to describe the reaction mechanism. A more accurate description of the momentum distribution was obtained by DWBA by using the FRESCO code [21] (dashed red line in Fig. 1, $\tilde{\chi}^2 = 0.77$). As the experimental momentum distribution is in arbitrary units, the maximum of the DWBA theoretical distribution has been scaled to the experimental data. The parameters of the potentials used in the FRESCO calculation were extrapolated from the Perey and Perey compilation [22] as there were
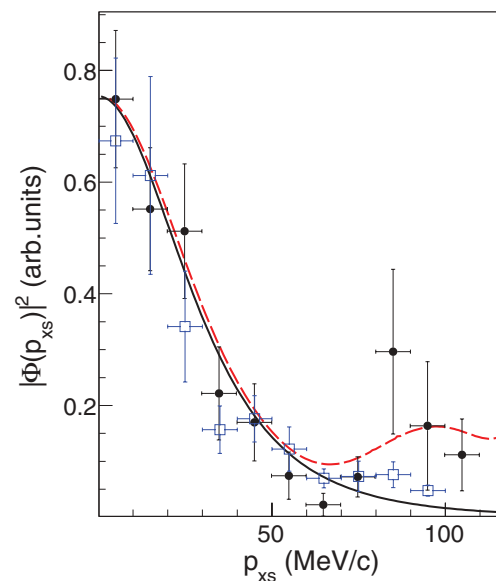

FIG. 1. (Color online) Experimental momentum distribution (full dots for the LNS experiment and open squares for the NSL experiment) compared with the Hulthén function (black solid line) and the distorted-wave Born approximation (DWBA) momentum distribution calculated by using the FRESCO code (red dashed line).

no available optical potentials at the low energies involved in the studied reaction. To check whether the uncertainty related to the choice of potential was comparable with the experimental one, FRESCO calculations were performed on varying the optical potential parameters in the entrance and exit channels by about 30% and by using the Koning-Delaroche optical potential [23] in the exit channel. Experimental data and FRESCO calculations are still in good agreement ($\tilde{\chi}^2 < 1.5$), even in these cases.

The comparison of DWBA and PWIA calculations with data shows good agreement by both theoretical distributions for $|p_{xs}| < 50$ MeV/c as distortions only influence the tails of the distribution. Indeed, for higher values of p_{xs}, the s cluster does not act as a spectator to the $A + x \rightarrow C + c$ reaction, and interactions in the final state must be taken into account [24,25]. In the following, only the events that have $|p_s| < 50$ MeV/c, for which the PWs constitute a viable approximation, are selected.

A further probe of the reliability of the PW approach in describing the experimental data comes from the comparison between PWBA and DWBA calculations. The differences in the ratios of the integrated resonance cross sections calculated in PW and DW approaches are less than 19%, compared with the experimental uncertainties (statistical $\sim$15% + fitting $\sim$14%). Therefore, as no absolute values of the cross sections are extracted, the PW description is used in the following.

The PWIA is generally preferred as it is less dependent from theory. In this approach, the three-body cross section assumes a simple expression from which the two-body cross section of interest is easily deduced

$$\frac{d^3\sigma}{dE_1 dE_2 d\Omega} \propto KF |\Phi(p_{xs})|^2 \sum_{l_1} |L_{l_1}|^2 \frac{d\sigma_{l_1}^{\text{HOES}}}{d\Omega}. \quad (1)$$

In Eq. (1), KF is a kinematical factor, which depends on masses, momenta, and angles of the outgoing particles, and it takes into account the final-state phase-space factor [1–8]. $\Phi(p_{xs})$ is the momentum distribution of the clusters in the TH nucleus. l_1 is the orbital momentum in the entrance channel A-x, and $|L_{l_1}|^2$ is a coefficient expressed in terms of the Wronskian of regular and outgoing solutions of the free radial Schrödinger equation, taken at the off-shell and on-shell x-A momenta correspondingly. $d\sigma_{l_1}^{\text{HOES}}/d\Omega$ is the half-off-energy-shell (HOES) cross section of the ^{17}O$(n, \alpha)^{14}$C reaction at the center-of-mass reaction angle $\theta_{\text{c.m.}}$ calculated as [26] $\theta_{\text{c.m.}} = \arccos(\hat{\mathbf{k}}_{Ax} \cdot \hat{\mathbf{k}}_{Cc})$, where $\mathbf{k}_{ij}$ is the relative momentum of the particles i and j, and $\hat{\mathbf{k}}_{ij} = \mathbf{k}_{ij}/k_{ij}$. The HOES label for the ^{17}O$(n, \alpha)^{14}$C cross section refers to the off-energy-shell nature of the transferred neutron.

The cross section of the ^{17}O$(n, \alpha)^{14}$C reaction was then extracted from Eq. (1) by dividing the experimental yield by the product $KF |\Phi(p_{xs})|^2$, estimated by means of a Monte Carlo simulation where the experimental momentum distribution shown in Fig. 1 was used. This introduces an uncertainty of 10% in the experimental data. Typical excitation functions for the ^{17}O $+ n$ reaction are shown in Fig. 2 in arbitrary units: Fig. 2(a) reports the LNS experimental data for $50° < \theta_{\text{c.m.}} < 60°$, and Fig. 2(b) shows the NSL experimental data
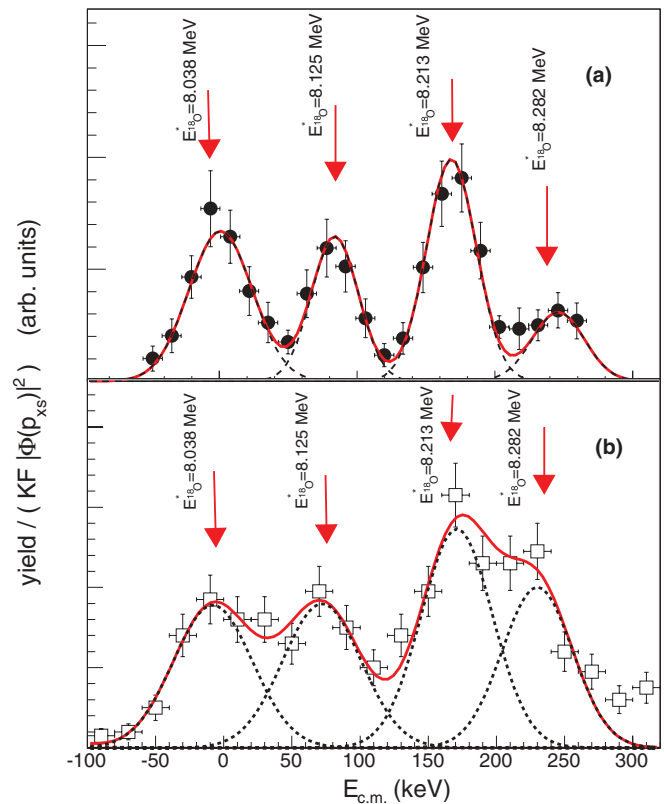

FIG. 2. (Color online) Excitation function of the ^{17}O$(n, \alpha)^{14}$C reaction from the LNS experiment (a) for $\theta_{\text{c.m.}} = 55° \pm 5°$ and from the NSL experiment (b) for $\theta_{\text{c.m.}} = 65° \pm 25°$. The red solid line is a fit, which uses four Gaussian functions; the black dashed lines represent their individual contributions.

for $40° < \theta_{\text{c.m.}} < 90°$. In the figure, the horizontal error bars represent the integration energy bin, and the vertical bars take into account the statistical uncertainties. The solid line represents the result of a fit performed using four Gaussian functions to disentangle the contributions of the four ^{18}O resonances populated in the explored energy and $\theta_{\text{c.m.}}$ range. No interference effect is taken into account in the fitting procedure, owing to the resonance widths ($<$15 keV), which are much smaller than their energy separations (see Table I). The use of a Gaussian function for fitting the contributions due to the resonances is justified by considering the energy resolution of the THM measurement as discussed in Ref. [6]. The width of the four resonances is the same and is equal to the experimental resolution $\sigma = 20$ keV for the LNS experiment and $\sigma = 30$ keV for the NSL experiment. The peak energies that come from the fit well reproduce the resonance energies compiled in Ref. [13] and are shown by arrows in Fig. 2.

The extracted two-body cross section does not suffer from the centrifugal barrier penetration effect. In particular, the presence of the level at $E^* = 8125 \pm 2$ keV, $J^\pi = 5^-$ must be noted. It has clearly been observed in both of the present experiments but was missed in the direct measurements. Since Coulomb effects are absent in neutron-induced reactions, it is directly evident from this result that only the pure nuclear

interaction potential enters into the virtual $A + x$ reaction studied by THM.

To confirm the spin assignment of the ^{18}O levels, the angular distributions for the four resonances were extracted. The experimental setup provided coverage of the c.m. angular ranges $\theta_{c.m.,1} = 0°–40°$, $\theta_{c.m.,2} = 30°–90°$, and $\theta_{c.m.,3} = 70°–100°$ with overlap regions among the three detector coincidences, which allowed for a relative normalization of the data. The contribution of each resonance to the overall coincidence, yielded at different angles $\theta_{c.m.}$, was disentangled by using a four-Gaussian fitting procedure as in Fig. 2. The obtained angular distributions in arbitrary units are shown in Fig. 3 as full dots for the LNS experiment and open squares for the NSL experiment. By following the formalism developed in Refs. [27,28] and by assuming that ^{17}O$(n, \alpha)^{14}$C is going through isolated compound levels of ^{18}O with spin J^π, the angular distributions for the free on-energy-shell reaction is given by

$$W(l_1, S_1, J, l_2, S_2; \theta_{c.m.}) \propto \sum_L Z(l_1 J l_1 J; S_1 L) Z(l_2 J l_2 J; S_2 L)$$
$$\times P_L(\cos \theta_{c.m.}), \quad (2)$$
$$Z(abcd; ef) = \widehat{a}\widehat{b}\widehat{c}\widehat{d} \langle ac00|acf0 \rangle R(abcd; ef).$$

Here, $P_L(\cos \theta_{c.m.})$ is the Legendre polynomial of order L; $\widehat{i} = (2i + 1)^{1/2}$; $\langle ac00|acf0 \rangle$ is the Clebsch-Gordan coefficient; $R(abcd; ef)$ is the Racah coefficient; $\mathbf{S}_1 = \mathbf{I}_A + \mathbf{s}_x$, where $\mathbf{I}_A$ and $\mathbf{s}_x$ denote the spins of target and projectile; $\mathbf{l}_1$ is the orbital momentum in the entrance channel, given by $\mathbf{J} = \mathbf{S}_1 + \mathbf{l}_1$; finally, $\mathbf{S}_2$ and $\mathbf{l}_2$ are the spin and orbital momentum in the exit channel. The solid lines in Fig. 3 represent the results of calculations for the populated resonances without any fitting parameter except for one free parameter to normalize the yields. The comparison between the experimental data and the calculation confirms that levels $E^* = 8038$ and 8282 keV are populated in $l_1 = 1$, and $E^* = 8125$ keV is populated in $l_1 = 3$. However, the angular distribution of the resonance, which corresponds to the $E^* = 8213$ keV level, is better reproduced by adopting $l_1 = 2$ (solid line, $\tilde{\chi}^2 = 0.82$) instead of $l_1 = 0$ (dashed line, $\tilde{\chi}^2 = 1.55$) as usually assumed by considering the low value of the neutron energy available in the c.m. system [29].

The differential cross section for the ^{17}O$(n, \alpha)^{14}$C reaction extracted from the THM measurements was then integrated over $\theta_{c.m.}$, which assumed the theoretical trend outside the angular range covered by the measurement. The uncertainty in the integration, which comes from the uncertainty on the fit parameters, is of 3%, 20%, 11%, and 8% for the resonances at energies $E^* = 8038$, 8125, 8213, and 8282 keV, respectively.

To compare the TH data with the direct measurements, the TH cross section is multiplied by the penetrability factor calculated for each resonance by $P_{l_1}(kr) = 1/[kr(j_{l_1}(kr)^2 + n_{l_1}(kr)^2)]$, where l_1 is deduced from the angular distribution, and $j_{l_1}(kr)$ and $n_{l_1}(kr)$ are the spherical Bessel and Neumann functions, respectively. The contribution of each resonance for a fixed value of energy is evaluated by fitting the TH cross section by using four Gaussian functions, which follows the same procedure used in Fig. 2. The reaction radius used
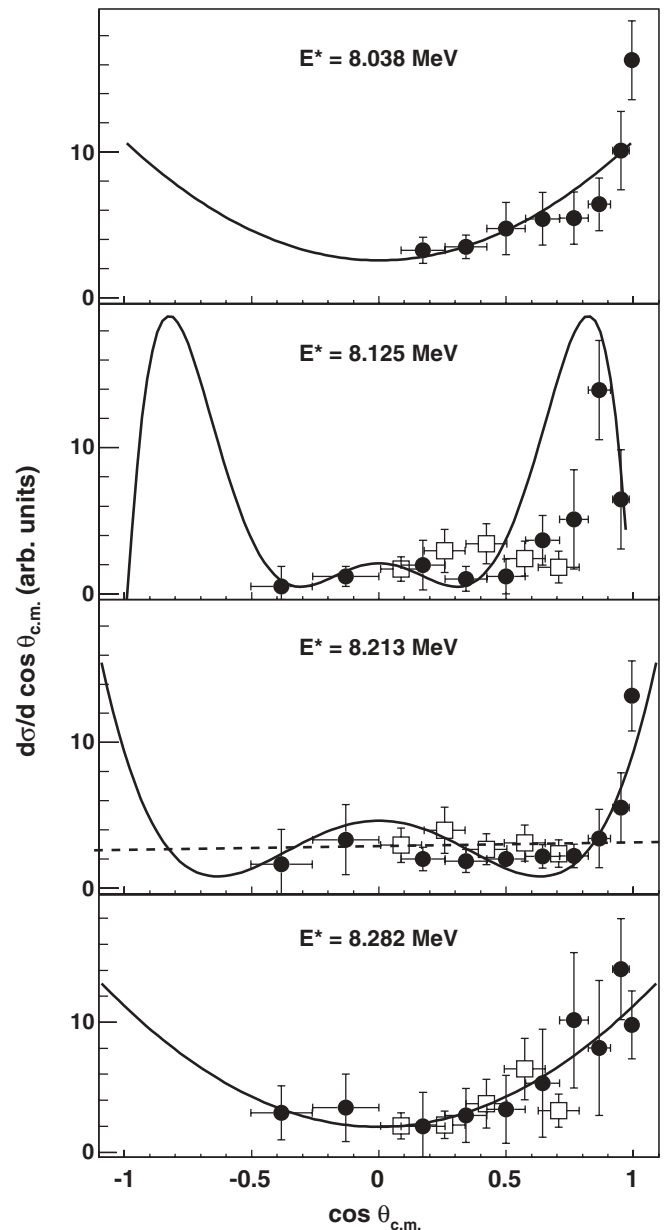

FIG. 3. Angular distributions for the ^{17}O$(n, \alpha)^{14}$C reaction for the four ^{18}O resonances populated in this Rapid Communication (full dots represent the LNS experiment, and open squares represent the NSL experiment) The solid lines are the theoretical angular distribution for the on-energy-shell reaction calculated as described in Refs. [27,28]. The dashed line for $E^* = 8213$ keV represents the angular distribution for $l_1 = 0$ as discussed in the text.

for the calculation of the penetrability factor was given by $R = r_0(17^{1/3})$, where $r_0 = 1.6$ fm. The change in the scaled cross sections is still inside the experimental uncertainties if $1.2 < r_0 < 1.9$. The result is shown in Fig. 4. For comparison, the direct data from Ref. [14] have been smeared to the THM experimental resolution, and they are shown, where available, as a solid line in Fig. 4. Moreover, the actual direct data from Ref. [14] are shown in Fig. 4 as a dashed red line (color online). The two data sets have been normalized at the maximum of the resonance at $E^* = 8213$ keV where indirect data have smaller
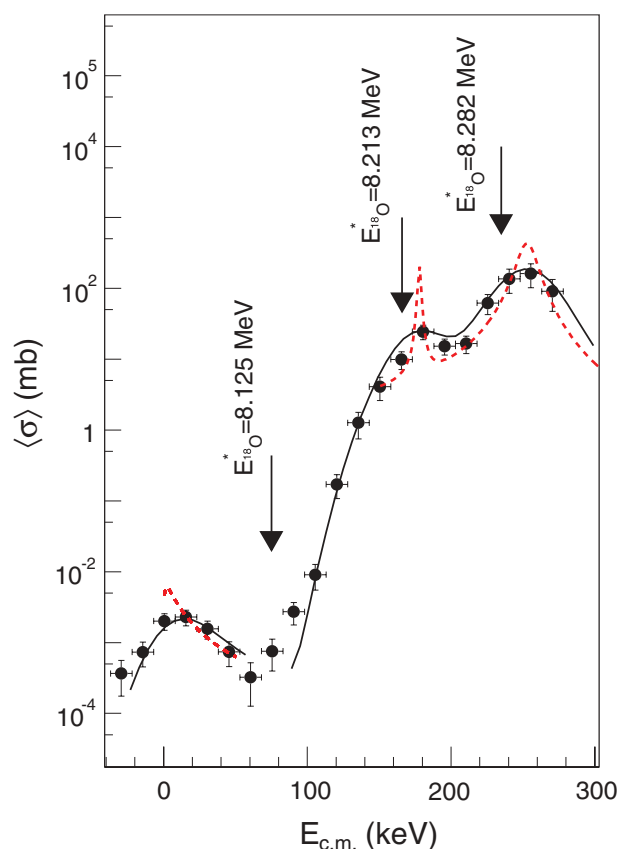
FIG. 4. (Color online) Cross section of the $^{17}O(n, \alpha)^{14}C$ reaction from TH data after the correction for the penetrability of the centrifugal barrier (full dots). The dashed red line represents the direct data from Ref. [14] where available, whereas, the solid line reports the direct data smeared at the TH energy resolution.

error bars. The widths of the peaks are determined by the TH data experimental resolution. The agreement between the two data sets is evident.

In conclusion, this measurement has demonstrated the ability of the THM to determine the nuclear structure parameter of orbital momentum-suppressed neutron capture resonances. This is evidenced by the population of the $J^{\pi} = 5^{-}$ level of ^{18}O, present in the indirect data for the neutron-induced reaction but not observed in direct neutron capture studies. This demonstrates the effectiveness of the THM to emphasize the mere nuclear interaction, which avoids the centrifugal suppressions or the electron screening effects, which opens new perspectives in the use of the method for nuclear structure studies. A particularly interesting application is the study of neutron-induced reactions on short-lived radioactive nuclei by using inverse kinematics. This approach will provide a unique method to study n-induced reactions on short-lived nuclei, which are crucial for both nuclear astrophysics and in nuclear engineering.

[1] S. Cherubini *et al.*, Astrophys. J. **457**, 855 (1996).
[2] C. Spitaleri *et al.*, Nucl. Phys. A **719**, C99 (2003).
[3] M. La Cognata *et al.*, Phys. Rev. C **76**, 065804 (2007).
[4] A. Tumino *et al.*, Phys. Rev. Lett. **98**, 252502 (2007).
[5] M. L. Sergi *et al.*, Phys. Rev. C **82**, 032801 (2010).
[6] M. La Cognata *et al.*, Astrophys. J. **708**, 796 (2010).
[7] L. Lamia *et al.*, J. Phys. G: Nucl. Part. Phys. **39**, 015106 (2012).
[8] M. Gulino *et al.*, J. Phys. G: Nucl. Part. Phys. **37**, 125105 (2010).
[9] M-S. Yim and F. Caron, Prog. Nucl. Energy **48**, 2 (2006).
[10] J. Applegate *et al.*, Astrophys. J. **329**, 572 (1988).
[11] M. Forestini and C. Charbonnel, Astron. Astrophys. Suppl. Ser. **123**, 241 (1997).
[12] L. R. Nittler *et al.*, Nucl. Phys. A **621**, 113c (1997).
[13] F. Ajzenberg-Selove, Nucl. Phys. A **475**, 1 (1987).
[14] J. Wagemans *et al.*, Phys. Rev. C **65**, 034614 (2002).
[15] H. Schatz *et al.*, Astrophys. J. **413**, 750 (1993).
[16] P. E. Koehler and S. M. Graff, Phys. Rev. C **44**, 2788 (1991).
[17] R. M. Sanders, Phys. Rev. **104**, 1434 (1956).
[18] Y. M. Gledenov *et al.*, Nucl. Instrum. Methods Phys. Res. Sect. A **431**, 201 (1999).
[19] J. Wagemans, C. Wagemans, G. Goeminne, and P. Geltenbort, Phys. Rev. C **61**, 064601 (2000).
[20] J. Wagemans, C. Wagemans, R. Bieber, and P. Geltenbort, Phys. Rev. C **58**, 2840 (1998).
[21] I. J. Thompson, Comput. Phys. Rep. **7**, 167 (1987).
[22] C. M. Perey and F. G. Perey, At. Data Nucl. Data Tables **17**, 1 (1976).
[23] A. J. Koning and J. P. Delaroche, Nucl. Phys. A **713**, 231 (2003).
[24] R. G. Pizzone *et al.*, Phys. Rev. C **71**, 058801 (2005)
[25] R. G. Pizzone *et al.*, Phys. Rev. C **80**, 025807 (2009).
[26] G. G. Ohlsen, Nucl. Instrum. Methods **37**, 240 (1965).
[27] J. M. Blatt and L. C. Biedenharn, Rev. Mod. Phys. **24**, 258 (1952).
[28] V. V. Ketlerov *et al.*, Nucl. Phys. A **621**, 243 (1997).
[29] J. A. Weinman and E. A. Silverstein, Phys. Rev. **111**, 277 (1958).